Boundary Shape Optimization Using the Material Distribution Approach

BY
FOTIOS KASOLIS

June 2011

DEPARTMENT OF COMPUTING SCIENCE, UMEÅ UNIVERSITY, UMEÅ, SWEDEN

TO MY BELOVED MOTHER STELLA

How could they force me face
The sun in a different way?
On its steps
My mother taught me (how) to live.

Kostantinos Kindinis – How could I stay silent

Cover picture source: `http://www.athenstourgreece.com/`. The ancient greek theater of Epidaurus.
Used with permission.

List of papers

The thesis consists of the following papers

1. F. Kasolis, E. Wadbro, M. Berggren. Avoiding mesh deformations in boundary shape optimization. Submitted to *Structural and Multidisciplinary Optimization*.
   Contributions. The author of the thesis contributed to all stages of the paper, from developing ideas to the actual implementation, as well as the manuscript preparation.

2. M. Berggren, F. Kasolis. Weak material approximation of holes with traction-free boundaries. Submitted to *SIAM Journal of Numerical Analysis*.
   Contributions. The author of the thesis is responsible for planning and performing the numerical experiments and for writing the corresponding section.

Chapter 1

Computational design optimization

1.1 Introduction

Designing efficient devices or mechanical components is an important step in the engineering process. In many cases, the physical properties of the object of interest depend on its geometric characteristics and can be controlled by varying its shape or its connectivity. *Computational design optimization* consists of those mathematical and computational tools that make feasible the numerical optimization of the geometric form of an object. An attractive feature of computational design optimization is that it is performed without the economical cost of manufacturing every suggested design. On the other hand, it is a computationally demanding field, and several issues arise in practical implementations that have prevented engineers from using it as a standard design tool. Due to the role of the geometric characteristics on the quality of the final product, we understand the gain of utilizing computational design optimization.

To effectuate computational design optimization, we start by choosing a flexible shape parameterization, and appropriate *design variables* are introduced. In addition, a function that measures the performance is also introduced. This *objective function* depends on the design variables and is to be extremized. The class of problems we are interested in can be formulated as optimization problems supplemented with partial differential equation (PDE) constraints. The PDE constraints govern the phenomena under investigation and are often referred to as the *state equations*. Additional side constraints may or may not be present, and the PDE problem is discretized to enable numerical solutions. The typical approach in solving the optimization problem starts with an initial design guess. The objective function value is then evaluated, and a new design, which better fulfills the desired properties, is suggested. An advantage with computational design optimization, compared to

manual, trial-and-error optimization, is that it can be used to optimize over a larger number of design variables than would otherwise be feasible.

Two major classifications of design optimization approaches, based on the design parameterization, are *boundary shape optimization* and *topology optimization*. In boundary shape optimization, we modify the boundary shape of a given domain, whereas in topology optimization, changes in the topology, such as the number of holes, are also admissible and are decided on during the optimization. Several methods have been proposed to perform topology optimization, such as the *material distribution method* [4] and the *level-set approach* [1]. In the former we directly optimize over a coefficient in the state equation such as the local material density, whereas in the later, shape derivatives are combined with level-set functions transported using a Hamilton–Jacobi equation to obtain an optimal design.

1.2 Boundary shape optimization

Boundary shape optimization traces its roots back to the classic subject of calculus of variations and can be tracked back to the works by Newton, Lagrange, and Hadamard. Boundary shape optimization in its modern form was initiated in the 1970s by, for instance, Cea, Glowinski, and Pironneau and has been applied, among other engineering fields, in fluid mechanics [14] as well as in acoustics [18].

The abstract boundary shape optimization problem can be formulated by defining an objective function $J(u(\Omega))$ that, through observations of a state function u that quantifies the physics, measures the performance of a given object occupying a domain Ω. In boundary shape optimization, the shape of Ω is specified by parameterizing its boundary $\partial\Omega$. The state function u is the solution to a state equation $S(u(\Omega)) = 0$, which can be incorporated into the optimization problem as a constraint, possibly together with additional side constraints. A crucial component in boundary shape optimization is the selection of a suitable parameterization of $\partial\Omega$. Some kind of splines can, for instance, be used, but a variety of choices is available as reviewed by Samareh [17]. An alternative to splines is to use the mesh nodes at the boundary as design variables in combination with some smoothing strategy to avoid shape fluctuations [13].

To solve the state equation $S(u(\Omega)) = 0$, we typically need to mesh a computational domain that borders Ω. During the optimization, the computational domain has to be re-meshed or the mesh has to be modified so that it conforms to the generated designs. Several mesh deformation algorithms have been proposed [12] and many of them share in common the idea of deforming the mesh as if it was an elastic structure. Mesh deformation algorithms are often prone to robustness problems. Moreover, in the case we wish to calculate exact gradients of the discrete objective function, we need to include sensitivities with respect to mesh deformations. Therefore, the presence of mesh deformations often leads to practical difficulties when performing boundary shape optimization. Our approach in paper I circumvents the re-meshing/deforming complexities by using a fixed-mesh approach that results in

raster representations of the designs similar as in the material distribution method presented below.

Boundary shape optimization problems can be solved using gradient-based methods such as sequential quadratic programming (SQP), Newton, or quasi-Newton methods. For a brief discussion about nonlinear optimization methods used in boundary shape optimization, the reader is pointed to chapter 4 of the book by Haslinger and Mäkinen [10]. The convergence of the optimization algorithm depends strongly on the accuracy of the derivatives, and for some problems, finite-difference schemes can be admissible. However, a less costly and more accurate method is the *adjoint method*. The adjoint method provides an efficient way to compute derivatives when the number of design variables is greater than the side constraints. Jameson [11] and Pironneau [16], among many others, have successfully applied the adjoint method in aerodynamics and fluid mechanics boundary shape optimization problems, respectively. Due to the structure of the problem studied in paper I, the solution to the adjoint state equation is proportional to that of the state equation itself. An alternative, black-box solution to sensitivity analysis is *algorithmic differentiation*, which provides a software that generates the exact values for the derivatives of the discrete objective function. For more information see chapter 8 of the book by Nocedal and Wright [15].

1.3 The material distribution method

The material distribution method is perhaps the most widely used approach for topology optimization, and it is an appealing method in the early stages of engineering design. The reason for this is the method's generality and ease of implementation. In the discrete setup, the resulting designs are represented using pixels, each one assigned a value $\rho(x) \in \{0,1\}$ that indicates the absence/presence of material, respectively. The value of each pixel is to be decided by the optimization; the material distribution function ρ is the design variable. The function ρ occurs as a varying coefficient in the state equation and typically represents a material property such as relative density. To avoid dealing with a computationally costly nonlinear integer optimization problem, we relax the design variables by allowing intermediate values, $\rho(x) \in [0,1]$, so that "shades of gray", $\rho(x) \in (0,1)$, are also part of the generated designs. To promote designs that approximate the solutions of the integer problem, some penalization method is usually needed. A penalty approach discussed by Allaire and Kohn [2] adds an explicit penalty term to the objective function, whereas an alternative approach modifies the material interpolation scheme. A material interpolation scheme commonly used for linear elasticity problems is SIMP (simple material with penalization), which changes the equations' varying coefficient from ρ to ρ^s, where $s > 1$ is a number chosen so that the intermediate $\rho(x)$ values result in designs with low stiffness compared to the mass used. For a review of material interpolation schemes in topology optimization we refer to Bensøe and Sigmund [3].

The use of penalty techniques to force the continuous design variable ρ to

approximate binary values typically leads to an ill-posed mathematical problem. One way to deal with this problem is to use regularization strategies such as *design restrictions*. Borrvall [5] reviews and compares several of the proposed regularization strategies, such as the *perimeter constraint method* and *filtering techniques*.

Bourdin [7] proves the well-posedness of the filtered optimization problem, whereas Borrvall and Petersson [6] provide a proof of the well-posedness of the optimization problem in the presence of filtering when the finite-element discretization is used. Moreover, filtering can be used to remove a certain type of numerical instability, the formation of checkerboard patterns [7, 8]. Note that in paper I there is no need for filtering since we do not directly optimize over pixel values.

The governing equations vanish in regions where $\rho = 0$, and the solution is undetermined in these regions. A common remedy for this problem is to replace the lower bound $\rho = 0$ by a small, positive number $\epsilon \ll 1$. In the finite element setup, this replacement yields a non-singular linear system $\mathbf{A}_\epsilon \mathbf{x} = \mathbf{f}$, where the condition number of the coefficient matrix $\mathbf{A}_\epsilon$ increases as ϵ approaches zero. The error that this ϵ perturbation introduces has been analyzed for scalar, elliptic problems, in the context of so-called fictitious domain methods, by Glowinski and Pan [9] and Zhang [19]. In paper II, we prove, for the linear elasticity problem, an error estimate regarding the ϵ approximation, and we provide bounds on the condition number of the finite-element stiffness matrix. Similar analysis for the Helmholtz problem of paper I is much more complicated due to the lack of coercivity of the state equation and still remains an open problem.

Chapter 2

Summary of Papers

2.1 Avoiding Mesh Deformations in Boundary Shape Optimization (paper I)

2.1.1 Introduction

We use a discrete curvature parameterization with a fictitious domain approach for representing and optimizing the shape of an acoustic horn and to avoid deforming the computational mesh. The optimization problem is to minimize the reflections back to a feeding waveguide. In other words, the optimal horns transmit most of the wave energy into free space. The design boundary consists of a predefined number of line segments of constant length, and the angles between consecutive line segments are chosen to be the design variables. In each step of the optimization, the current design domain is mapped onto the computational mesh using an exact area-coverage algorithm. The resulting geometries are represented through varying coefficients in the governing equations.

By performing a variety of experiments, using different numbers of segments, we conclude that the number of segments is not significant in the sense that refined descriptions of the design boundary yield designs that appear to converge with increasing number of segments in most of the cases we examined. In addition, the parameterization inherently promotes smooth designs without unduly restriction of the design flexibility. The optimized, smooth horns consistently show favorable transmission properties.

2.1.2 Problem setup

The problem we are interested in is to optimize the shape of a planar symmetric horn in free space with respect to reflections measured at a waveguide attached to the horns throat. For that purpose, a two-dimensional acoustic wave propagation problem is solved in the frequency domain. The governing boundary value

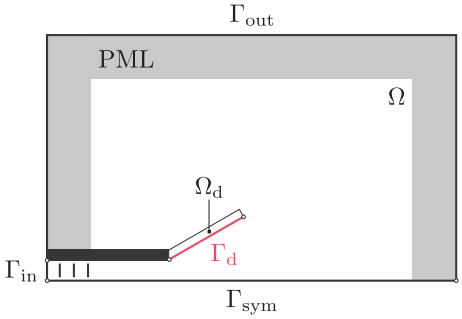

Figure 2.1: The computational configuration for the horn problem.

problem consists of the Helmholtz equation combined with appropriate boundary conditions.

The computational domain $\hat{\Omega}$ is the union of the horn domain Ω_{d} and the free-space domain Ω (figure 2.1) . The variational form that also incorporates the varying coefficients for describing the horn domain Ω_{d} reads

$$\begin{aligned} &\text{find } p_h^k \in V_h \subset H^1(\hat{\Omega}) \text{ such that} \\ &\int_{\hat{\Omega}} \alpha_h \nabla q_h \cdot (\mathbf{D}_h \nabla p_h^k) - k^2 \int_{\hat{\Omega}} \alpha_h \gamma_h q_h p_h^k \\ &+ \mathrm{i}k \int_{\Gamma_{\text{in}}} q_h p_h^k = 2\mathrm{i}kA \int_{\Gamma_{\text{in}}} q_h, \quad \forall q_h \in V_h, \end{aligned} \tag{2.1}$$

where V_h is the space of continuous, element-wise bi-quadratic functions, Γ_{in} denotes the truncated waveguide boundary, α_h are the coefficients that represent the horn domain Ω_{d}, γ_h and $\mathbf{D}_h$ are quantities related to a perfectly matched layer used to impose the non-echoic character of $\hat{\Omega}$, k is the wave number of the propagating wave, and A the complex amplitude of a right-going wave within the waveguide. By introducing a generic parameterization with design variables ϑ, and assuming that the values α_h depend on ϑ, the optimization problem we are interested in is formulated as the minimization of the reflections back to the feeding waveguide. That is

$$\min_{\vartheta} \frac{1}{2} \sum_{k \in \mathrm{K}} J_k^2(\alpha_h(\vartheta)), \tag{2.2}$$

where

$$J_k(\alpha_h(\vartheta)) = \frac{|\langle p_h^k \rangle_{\text{in}} - A|}{|A|}. \tag{2.3}$$

The set K consists of the wavenumbers we optimize for, and $\langle p_h^k \rangle_{\text{in}}$ is the average value of the solution p_h^k to (2.1) on the boundary Γ_{in}.

2.1.3 Design Boundary Parameterization

Let Γ_{d} be the boundary subject to optimization. We define Γ_{d} as a set of connected line segments, all of length ℓ, that comprise a polygonal line. Each line segment is

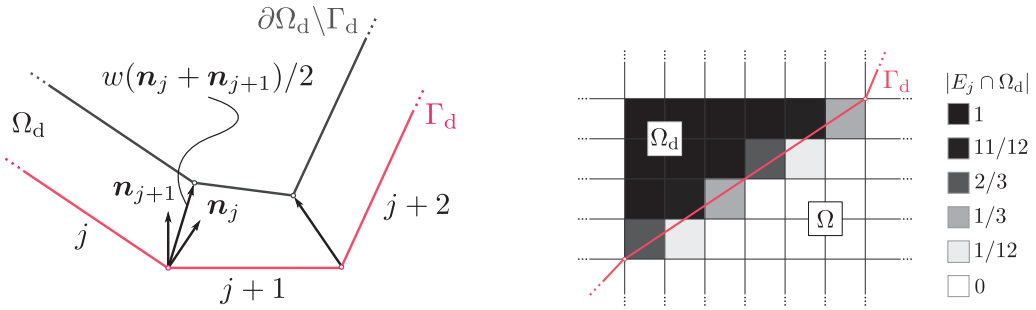

Figure 2.2: (Left) The back side of the horn is generated by linear interpolation of the points $w(\mathbf{n}_j+\mathbf{n}_{j+1})/2$. (Right) The values of the area $|E_n\cap\Omega_\mathrm{d}|$ used to find the values α_n of the function α_h.

characterized by the angle difference ϑ_j, between segments $j-1$ and j, $j=1,2,\ldots,S$. We note that ϑ_j/ℓ is the discrete curvature of Γ_d.

Given the above described boundary parameterization, we construct the design domain Ω_d by generating the points $w(\mathbf{n}_j+\mathbf{n}_{j+1})/2$, where w is the width of the material that forms the waveguide and $\mathbf{n}_j$ are the normals to the line-segments comprising Γ_d. We choose not to separately parameterize the back side $\partial\Omega_\mathrm{d}\backslash\Gamma_\mathrm{d}$ of the horn since computational experience suggests that the effect of its shape on the objective function is insignificant compared to that of Γ_d. The design domain Ω_d is then mapped onto the computational mesh by assigning to each element E_n a value according to the formula

$$\alpha_h|_{E_n}=\alpha_n=1+(\varepsilon-1)\frac{|E_n\cap\Omega_\mathrm{d}|}{|E_n|}, \tag{2.4}$$

where $|\cdot|$ denotes the area occupied by the corresponding set and $0<\varepsilon\ll 1$ is a parameter that characterizes the sound-hard material in Ω_d. Equation (2.4) interpolates between the values 1 and ε based on the relative portion of each element E_n that lies within Ω_d. By doing so, the geometry enters the governing equations as varying coefficients. We note that elements for which $E_n\cap\Omega_\mathrm{d}=\emptyset$ are assigned the value $a_h=1$ meaning that the wave propagation problem remains unchanged within $\hat{\Omega}\backslash\Omega_\mathrm{d}$, whereas elements for which $E_n\cap\Omega_\mathrm{d}=E_n$ are assigned the value $a_h=\varepsilon$. The small positive value ε is chosen different than zero to avoid the formation of singular matrices.

2.1.4 Selected results

The formulated optimization problem is a non-linear least squares problem solved using Matlab's routine `lsqnonlin`. The weak material parameter is chosen to be $\varepsilon=10^{-8}$ after a comparison study with body-fitted geometry description implemented in FreeFem++. We perform experiments using 16, 32, and 64 line segments (design variables) for describing the design boundary Γ_d. Figure 2.3 depicts horns optimized for a single frequency of 200 Hz and their corresponding spectra. We observe that all

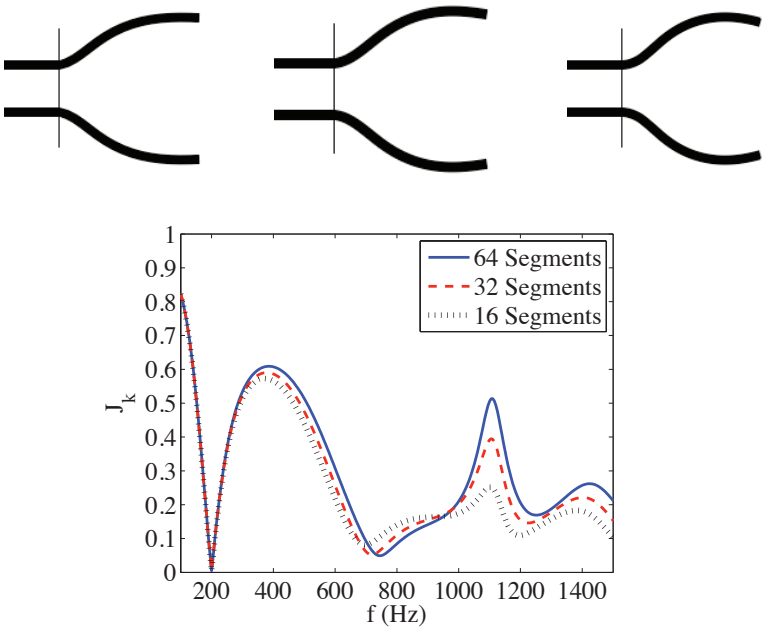

Figure 2.3: Optimal horns (top) with respect to reflections for a single frequency of 200 Hz and their corresponding spectra (bottom). The presented pixel representations correspond (from left to right) to 16, 32, and 64 design variables and the horn length is $|\Gamma_d|$ =0.4 m in all cases.

the designs perform remarkably good for the frequency we optimize for, and that they have similar spectra in the neighborhood of those frequencies. Moreover, we note that the horn is small (0.4 m) compared to the wave length when optimizing for 200 Hz (wavelength 1.725 m at speed of sound 345 m/s), which is why the spectra of those horns have poor transmission properties for frequencies other than the design frequency 200 Hz.

As a second example we present the results of a multi-frequency optimization experiment in figure 2.4. The horns are optimized for minimum reflections over the band of frequencies 466–1480 Hz. In this higher frequency range, it is easier to obtain horns with good transmission properties, compared to the 200 Hz case, since the horn here is larger measured in wave lengths. Here we see that the raster representations of the horns are very similar and the same holds for their reflection spectra, independent from the number of segments, whereas at the same time all those horns transmit energy remarkably well over the band of frequencies we optimize for.

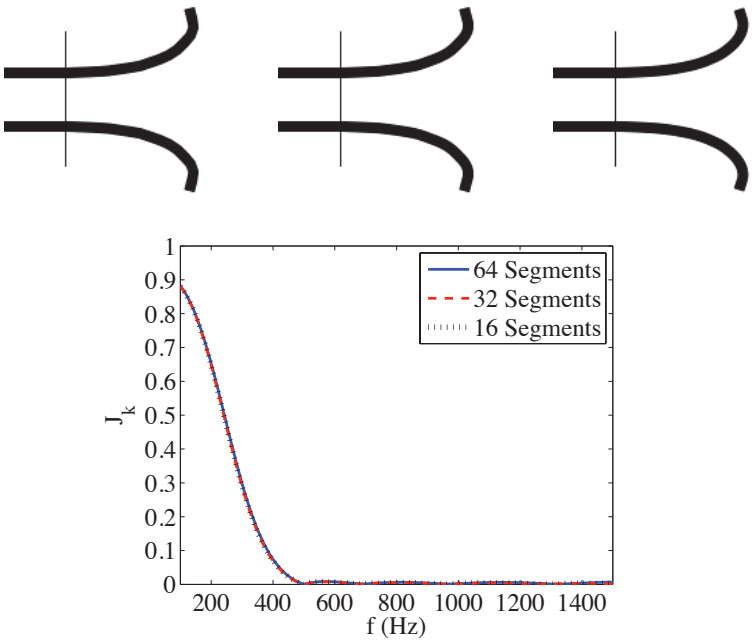

Figure 2.4: Optimal horns (top) with respect to reflections for 466–1480 Hz and their corresponding spectra (bottom). The presented pixel representations correspond (from left to right) to 16, 32, and 64 design variables and the horn length is $|\Gamma_d|$ =0.4 m in all cases.

2.2 Weak material approximation of holes with traction-free boundaries (paper II)

2.2.1 Introduction

The material distribution method for topology optimization, described in section 1.3, introduces a so-called material indicator function ρ with values $\rho \in \{0,1\}$, in the state equation. To avoid an undetermined solution within the material-free regions, the value $\rho = 0$ is routinely replaced by $\rho = \epsilon$, where $0 < \epsilon \ll 1$.

In this paper, we study the effect of the so-called weak-material parameter ϵ for a finite-element approximation of the linear elasticity problem. We prove that the weak material approximation introduces an error that is $O(\epsilon^{1/2})$ and also depends on the finite-element discretization. To obtain an approximation reasonably close to that of the original problem, ϵ has to be sufficiently small, a choice that results in finite-element matrices with large condition numbers. We show that the condition number of the finite-element stiffness matrix is proportional to ϵ^{-1}, and we also provide a preconditioner that makes the condition number independent from the weak-material parameter ϵ. Numerical computations that affirm the theoretical results are also included.

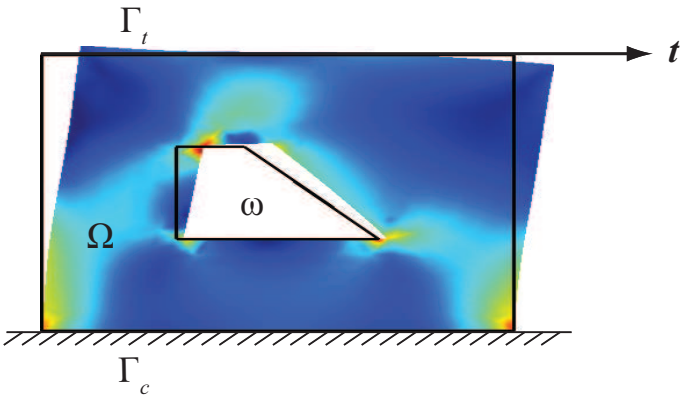

Figure 2.5: The model setup consists of an elastic structure containing a hole ω.

2.2.2 The elasticity problems

The standard variational form of the linear elasticity problem for a domain Ω with a traction-free hole ω, figure 2.5, reads

$$\begin{aligned} &\text{find } \mathbf{u} \in \mathbf{V} \text{ such that} \\ &\int_{\Omega} \nabla \mathbf{v} \cdot \mathbf{E} \nabla \mathbf{u} = \int_{\Gamma_t} \mathbf{v} \cdot \mathbf{t} \qquad \forall \mathbf{v} \in \mathbf{V}, \end{aligned} \tag{2.5}$$

where Ω is the domain of interest, $\mathbf{E}$ is the fourth-order elasticity tensor, $\mathbf{t}$ is the surface traction applied on $\Gamma_t \subset \partial\Omega$, and $\mathbf{V} = \{\mathbf{v} \in \mathbf{H}^1(\Omega) \mid \mathbf{v}|_{\Gamma_c} = \mathbf{0}\}$, where $\Gamma_c \subset \partial\Omega$. By introducing the material indicator function ρ, with values $\rho = 1$ in Ω and $\rho = 0$ in the hole ω, the above problem can be reformulated as

$$\begin{aligned} &\text{find } \mathbf{u} \in \hat{\mathbf{V}} \text{ such that} \\ &\int_{\hat{\Omega}} \rho \nabla \mathbf{v} \cdot \mathbf{E} \nabla \mathbf{u} = \int_{\Gamma_t} \mathbf{v} \cdot \mathbf{t} \qquad \forall \mathbf{v} \in \hat{\mathbf{V}}, \end{aligned} \tag{2.6}$$

where $\hat{\Omega} = \Omega \cup \omega$ and $\hat{\mathbf{V}} = \{\mathbf{v} \in \mathbf{H}^1(\hat{\Omega}) \mid \mathbf{v}|_{\Gamma_c} = \mathbf{0}\}$. Note that the state equation vanishes whithin the hole where $\rho = 0$, meaning that the finite-element matrices become singular and the solution undetermined within the hole. A common practice to circumvent this obstacle is to replace the value $\rho = 0$ with a small positive number $\rho = \epsilon \ll 1$. This approach is the so-called weak-material approximation. The discrete variational form of the weak-material approximation problem reads

$$\begin{aligned} &\text{find } \hat{\mathbf{u}}_h^{\epsilon} \in \hat{\mathbf{V}}_h \text{ such that} \\ &\int_{\Omega} \nabla \mathbf{v} \cdot \mathbf{E} \nabla \hat{\mathbf{u}}_h^{\epsilon} + \epsilon \int_{\omega} \nabla \mathbf{v} \cdot \mathbf{E} \nabla \hat{\mathbf{u}}_h^{\epsilon} = \int_{\Gamma_t} \mathbf{v} \cdot \mathbf{t} \qquad \forall \mathbf{v} \in \hat{\mathbf{V}}_h, \end{aligned} \tag{2.7}$$

where $\hat{\mathbf{V}}_h$ is the space of finite-element functions.

2.2.3 Error and condition number bounds

The use of the weak-material approximation results in a problem with a solution $\hat{\mathbf{u}}_h^\epsilon$ that approximates the solution $\mathbf{u}$ outside of the holes, that is $\hat{\mathbf{u}}_h^\epsilon|_\Omega \approx \mathbf{u}$. More precisely, there is a positive constant C such that the solution $\hat{\mathbf{u}}_h^\epsilon$ of the weak-material approximation problem satisfies

$$\begin{aligned} C\|\mathbf{u}-\hat{\mathbf{u}}_h^\epsilon\|_{H^1(\Omega)} \leq & \inf_{\mathbf{v}_h\in\hat{\mathbf{V}}_h} \|\mathbf{u}-\mathbf{v}_h\|_{H^1(\Omega)} \\ & + \epsilon^{1/2}\inf_{\mathbf{v}_h\in\hat{\mathbf{V}}_h} \|\mathbf{u}^\omega-\mathbf{v}_h\|_{H^1(\omega)} + \epsilon\left\|\lambda(\mathbf{u}^\omega)\right\|_{H^{-1/2}(\partial\omega)}, \end{aligned} \tag{2.8}$$

where $\mathbf{u}$ is the solution to the original problem (2.5), $\mathbf{u}^\omega$ is the continuous elastic extension of $\mathbf{u}$ into ω, and $\lambda(\mathbf{u}^\omega)$ is the surface traction on $\partial\omega$ from inside ω.

Problem (2.7) is discretized using the finite-element method by expanding functions $\mathbf{v}_h \in \hat{\mathbf{V}}_h$ in a basis $\boldsymbol{\phi}_i$ that consists of piecewise polynomials,

$$\mathbf{v}_h = \sum v_i \boldsymbol{\phi}_i \tag{2.9}$$

We denote by $\mathbf{A}_\epsilon$ the stiffness matrix of the resulting linear system. For quasi-uniform meshes, we show that the condition number $\kappa(\mathbf{A}_\epsilon)$ depends on the weak material parameter $\epsilon \in (0, 1/2]$ as

$$\kappa(\mathbf{A}_\epsilon) \leq Ch^{-2}\epsilon^{-1}, \tag{2.10}$$

where $h \in (0,1]$ is the mesh parameter, and C a constant. Moreover, we partition the nodal values $\mathbf{v}_h$ into vectors $\mathbf{v}_\Omega$, $\mathbf{v}_\Gamma$, and $\mathbf{v}_\omega$ with nodal values at nodes in Ω, Γ, and ω, respectively. By introducing the scaling matrix

$$\mathbf{D}_\epsilon = \mathrm{diag}(\mathbf{I}_{N_\Omega},\, (1+\epsilon)\mathbf{I}_{N_\Gamma},\, \epsilon\mathbf{I}_{N_\omega}), \tag{2.11}$$

where N_Ω, N_Γ, N_ω denote the lengths of the vectors $\mathbf{v}_\Omega$, $\mathbf{v}_\Gamma$, and $\mathbf{v}_\omega$, respectively, we show that the condition number $\kappa(\mathbf{D}_\epsilon^{-1}\mathbf{A}_\epsilon)$ is bounded independent of the weak material parameter ϵ as

$$\kappa(\mathbf{D}_\epsilon^{-1}\mathbf{A}_\epsilon) \leq Ch^{-2}. \tag{2.12}$$

Note that the limit matrix $\tilde{\mathbf{A}}_0 = \lim_{\epsilon\to 0}\mathbf{D}_\epsilon^{-1}\mathbf{A}_\epsilon$ is well desfined.

The following numerical experiments are performed to affirm the error estimate (2.8) and the bounds (2.10) and (2.12) regarding the non-preconditioned and the preconditioned stiffness matrices respectively. We consider the domain shown in figure 2.6, in which the material region is assumed to consist of a homogenous and isotropic elastic material.

We solve problem (2.5) using the fine triangulation shown in figure 2.6 and we denote its solution with $\mathbf{u}_{\mathrm{ref}}$. Moreover, both the non-preconditioned and the preconditioned problems are solved over the extended domains shown in figure 2.7 using the weak material approximation. The preconditioned problem is the one used when performing the error-estimate computations.

In figure 2.8 we observe that the semi-norm error $|\mathbf{u}_{\mathrm{ref}}-\mathbf{u}_h^\epsilon|_{H^1(\Omega)}$ is dominated by the presence of the weak material for large ϵ values. In addition, the slope of the

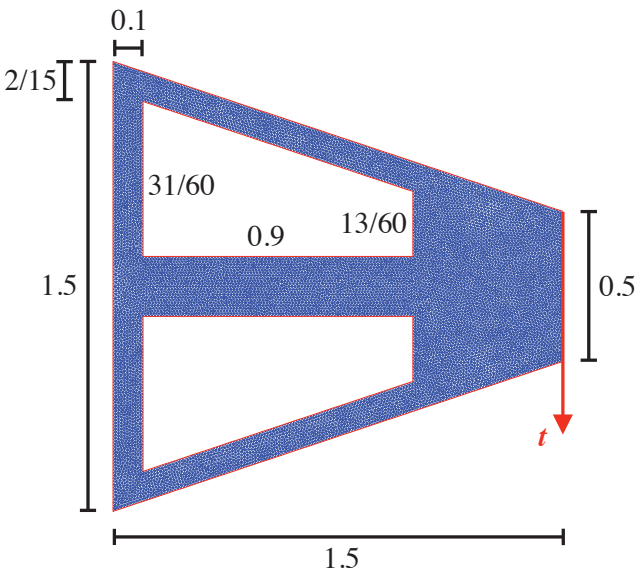

Figure 2.6: The triangulated domain, $h \approx 0.015$, used to obtain the reference solution $\mathbf{u}_{\text{ref}}$.

error curve is steeper for the finer mesh, and agrees well with the $O(\epsilon^{1/2})$ bound. For $\epsilon \leq 10^{-4}$, the error is dominated by the finite-element error term $O(h)$. Note that to avoid dominance of the $O(\epsilon^{1/2})$ term, fine meshes have to be used.

Figure 2.9 shows the dependence of the condition numbers $\kappa(\mathbf{A}_\epsilon)$ and $\kappa(\tilde{\mathbf{A}}_\epsilon)$ on the weak material parameter ϵ. We see that the condition number of matrix $\mathbf{A}_\epsilon$ grows proportional to ϵ^{-1}. For $\epsilon = 0$ the solution inside the holes becomes undetermined and the matrix $\mathbf{A}_0$ is singular. However, the condition number $\kappa(\tilde{\mathbf{A}}_\epsilon)$ is bounded independently of ϵ, and thus well conditioned as $\epsilon \to 0$.

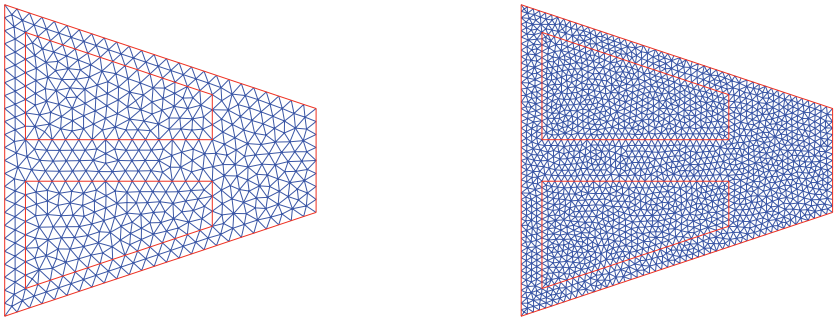

Figure 2.7: Extended domains and their triangulations, with $h \approx 0.082$ (left) and $h \approx 0.045$ (right), used for solving the problem (2.7).

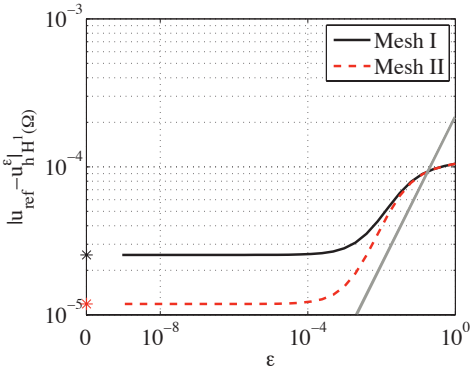

Figure 2.8: The error $|\mathbf{u}_{\text{ref}} - \mathbf{u}_h^\epsilon|_{H^1(\Omega)}$ as a function of ϵ for the two meshes shown in figure 2.7. The slope of the light colored straight line corresponds to $O(\epsilon^{1/2})$.

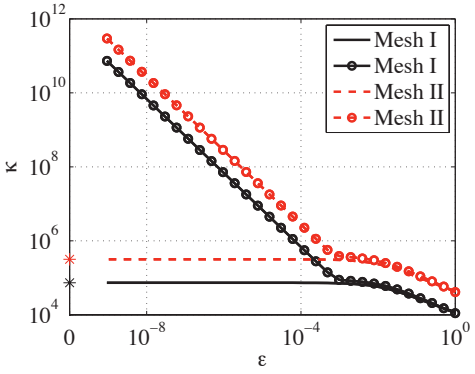

Figure 2.9: The condition number of the non-preconditioned (circles) as well as the preconditioned (solid and dashed lines) matrices as a function of the weak material parameter ϵ. The asterisks indicate the condition numbers for $\epsilon = 0$ when the preconditioned matrix is used.

Acknowledgments

I would like to express my gratitude to my scientific advisors Martin Berggren and Eddie Wadbro. It is not only their scientific expertise, but also their constant support, their patience, their understanding, and their humanity that were encouraging my faith and were lifting my sometimes weak spiritual motivation. I would also like to thanks Martin Berggren for giving me this opportunity that reformulated my whole existence.

Between all of my colleagues, who I all thank for a pleasant working environment, I want to point the very crucial and special place that Yvonne will always have in my heart. She made the difficult days in Umeå so much brighter and balanced, just as her beloved daughter Fanny did.

My family. What could I say about my family? There is no choice in my life that was not supported by them; bad or good, proper or improper. The only thing I was always receiving from them is love and endless understanding. I thank them for making me a person with values, human feelings, and weaknesses. I want to refer to my soul sisters Chryssa and Maria as my bright guides throughout my life's path. Their actions and reactions tought me a lot; their emotions make me feel secure and invulnerable when needed.

Fotios Kasolis
June 8, 2011

Bibliography

[1] Allaire, G., Jouve, F., Toader, A.M.: Structural optimization using sensitivity analysis and a level-set method. Journal of Computational Physics **194**, 363 – 393 (2004). DOI 10.1016/j.jcp.2003.09.032

[2] Allaire, G., Kohn, R.V.: Topology optimization and optimal shape design using homogenization. In: M. P. Bendsøe and C. A. Mota Soares (ed.) Topology design of structures, vol. 227, pp. 207–218 (1993)

[3] Bendsøe, M.P., Sigmund, O.: Material interpolation schemes in topology optimization. Archive of Applied Mechanics **69**, 635–654 (1999). DOI 10.1007/s004190050248

[4] Bendsøe, M.P., Sigmund, O.: Topology optimization. Theory, methods, and applications. Springer (2003)

[5] Borrvall, T.: Topology optimization of elastic continua using restriction. Archives of Computational Methods in Engineering **8**, 351–385 (2001)

[6] Borrvall, T., Petersson, J.: Topology optimization using regularized intermediate density control. Computer Methods in Applied Mechanics and Engineering **190**, 4911–4928 (2001). DOI 10.1016/S0045-7825(00)00356-X

[7] Bourdin, B.: Filters in topology optimization. International Journal for Numerical Methods in Engineering **50**, 2143–2158 (2001). DOI 10.1002/nme.116

[8] Bruns, T.E., Tortorelli, D.A.: Topology optimization of non-linear elastic structures and compliant mechanisms. Computer Methods in Applied Mechanics and Engineering **190**, 3443–3459 (2001). DOI 10.1016/S0045-7825(00)00278-4

[9] Glowinski, R., Pan, T.W.: Error estimates for fictitious domain/penalty/finite element methods. Calcolo **29**, 125–141 (1992)

[10] Haslinger, J., Mäkinen, R.A.E.: Introduction to shape optimization. SIAM (2003)

[11] Jameson, A., Martinelli, L., L., Pierce, N.A.: Optimum aerodynamic design using the Navier–Stokes equations. Theoretical and Computational Fluid Dynamics **10**, 213–237 (1998). URL `http://dx.doi.org/10.1007/s001620050060`

[12] Laporte, E., Tallec, P.L.: Numerical Methods in Sensitivity Analysis and Shape Optimization. Birkhäuser (2003)

[13] Mohammadi, B., Pironneau, O.: Applied shape optimization for fluids. Oxford science publications (2001)

[14] Mohammadi, B., Pironneau, O.: Shape optimization in fluid mechanics. Annual review of fluid mechanics **36**, 255–279 (2004). DOI 10.1146/annurev.fluid.36.050802.121926

[15] Nocedal, J., Wright, S.J.: Numerical optimization. Springer-Verlag (2006)

[16] Pironneau, O.: On optimum design in fluid mechanics. Journal of fluid mechanics (1974). DOI 10.1017/S0022112074002023

[17] Samareh, J.A.: A survey of shape parameterization techniques. Tech. rep. (1999)

[18] Udawwalpola, R., Berggren, M.: Optimization of an acoustic horn with respect to efficiency and directivity. International journal for numerical methods in engineering **73**, 1571–1606 (2007). DOI 10.1002/nme.2132

[19] Zhang, Z.: A domain embedding method for mixed boundary value problems. Comptes Rendus Mathematique **343**, 287–290 (2006). DOI 10.1016/j.crma.2006.06.025